View Article Online / Journal Homepage / Table of Contents for this issue
Dynamic Article Links

NJC

Cite this: *New J. Chem.*, 2011, **35**, 1898–1905

www.rsc.org/njc

PAPER

Structural and electrochemical characterization of metallo-porphyrins intercalated into ZnCr-layered double hydroxides: some evidence of dimer formation†

Christine Taviot-Guého,[a] Matilte Halma,[b] Khaled Charradi,[a] Claude Forano[a] and Christine Mousty*[a]

Received (in Montpellier, France) 9th May 2011, Accepted 21st June 2011
DOI: 10.1039/c1nj20400a

In this study, inorganic–organic hybrids were prepared by intercalation of metal complexes (Zn and Fe) of 5,10,15,20-tetrakis(4-sulfonatophenyl)porphyrin (TSPP) into Zn_2Cr layered double hydroxides (LDH) by coprecipitation method at constant pH. The resulting materials were characterized by powder X-ray diffraction, UV-Vis and FTIR spectroscopies showing the intercalation of porphyrins between the ZnCr layers. While monomer species are intercalated in the case of Zn_2Cr-ZnTSPP, the intercalation of dimers is likely to occur in the case of Zn_2Cr-FeTSPP. In both materials, a perpendicular orientation of the porphyrin ring against the hydroxide layers is proposed. Of particular interest is the good stability of ZnCr-LDH host over a wide pH range. The electrochemical behavior of these hybrid materials in both neutral (pH 7.0) and acid media (pH 4.5) was investigated by cyclic voltammetry. Zn_2Cr-FeTSPP exhibits an electrocatalytic activity for the reduction of oxygen, hydrogen peroxide and nitrite.

1. Introduction

Layered double hydroxides (LDH) are synthetic solids with positively charged brucite-like layers of mixed metal hydroxides separated by interlayer hydrated anions, defined by the general formula $[M^{II}{}_{1-x}M^{III}{}_x(OH)_2]^{x+}$ $[(A^{n-})_{x/n}\cdot yH_2O]$ (abbreviated as $M^{III}M^{II}$-A, where M^{II} and M^{III} are respectively divalent and trivalent metals, *R* corresponds to the M^{II}/M^{III} mole ratio ($R = (1 - x)/x$), and A^{n-} is the interlayer anion compensating the positive charge of the metal hydroxide layers). The increasing interest in LDH as host matrix arises from their versatile properties in terms of chemical composition of both layer and interlayer, their high and tuneable layer charge density resulting in adaptable anion exchange capacity. Hence, these materials are often used as immobilization matrices of organic anions, macromolecules or biomolecules.[1–3] These organic-inorganic hybrid materials have been developed for various application fields,[4] including pharmaceutical, cosmetic, sensors, photoreactive devices, *etc.*

Functionalization of inorganic host solids by porphyrins and metalloporphyrin complexes is under intensive investigations due to their unique catalytic, photochemical and electrochemical properties, which make porphyrin based hybrid materials potential candidates for applications in the development of novel catalysts,[5] light-harvesting photovoltaic systems,[6] optoelectronic devices,[7] and sensors.[8]

In 1989, Park *et al.* have prepared for the first time a porphyrin-LDH intercalation compound.[9] Since then, several publications have been focused on the intercalation of metalloporphyrins, bearing anionic groups, particularly in LDH hosts, pointing out the advantages of this type of hybrid materials for oxidation catalysis[10–14] and photochemistry.[15–20] Hence various free bases and metal-coordinated porphyrins were immobilized in LDH, such as 5,10,15,20-tetrakis(carboxyphenyl)porphyrins (*p*TCPP and *o*TCPP),[14,21] 5,10,15,20-tetrakis(4-sulfonatophenyl)-porphyrin (TSPP[17,22]) ant its metal complexes (ZnTSPP,[23] PdTSPP,[16,24] MnTSPP,[13,25,26] CoTSPP,[27] FeTSPP,[14,28] O=Ti^{IV}TSPP[18]), iron(III) complexes of 5,10,15,20-tetrakis(2,6-difluoro-3-sulfonatophenyl)porphyrin (FeTDFSPP), 5,10,15,20-tetrakis(2,6-dichloro-3-sulfonatophenyl)porphyrin (FeTDCSPP) and 5,10,15,20-tetrakis(2-chloro-6-fluoro-3-sulfonatophenyl)-porphyrin (FeTCFSPP).[12,29]

The LDH host compositions used for the intercalation of porphyrins have so far mostly been MgAl and ZnAl.[23] The intercalation of these negatively charged macrocycles into the LDH structures is generally achieved by conventional anion exchange of pre-formed LDH,[9,26,30] calcination/restacking method,[12,13,31,32] direct coprecipitation procedure.[11,18,21,23]

---

[a] *Clermont Université, Université Blaise Pascal, Laboratoire des Matériaux Inorganiques, CNRS UMR 6002, F-63171 AUBIERE, France. E-mail: Christine.Mousty@univ-bpclermont.fr; Fax: +33 473407108; Tel: +33 473407598*
[b] *Université Joseph Fourier, Département de Chimie Moléculaire, CNRS UMR 5250, F-38041 GRENOBLE, France*

† Electronic supplementary information (ESI) available: UV-Vis spectra of FeTSPP in solutions; X-ray powder diffraction patterns in the 2θ range 5–65° (inset 1–30°) of Zn_2Cr-ZnTSPP and Zn_2Cr-FeTSPP; FTIR spectra of Zn_2Cr-ZnTSPP and Zn_2Cr-FeTSPP and cyclic voltammograms in different buffer solutions. See DOI: 10.1039/c1nj20400a

More sophisticated methods using exfoliated hybrid LDH phases (MgAl-glycinate and MgAl-dodecylsulfate) were also reported for exchange or chemical grafting reactions with porphyrins.[33,34] Moreover, nano-ordered hybrid films of LDH nanosheets, TCPP and pyrenetetrasulfonic acid (PTSA) were prepared by a layer-by-layer deposition method.[35]

The interlayer confinement of porphyrinic macrocycles has been investigated as regard to guest ordering, microporosity and inner site accessibility, three key structural properties that determine material performances. It has been reported that free base porphyrins are intercalated with a selective orientation depending on the isomeric position of the anionic groups, *p*TCPP *versus* *o*TCPP for instance.[21] A perpendicular arrangement of macrocycles with respect to the hydroxide layer is obtained with the *para* carboxylate and *para* sulfonate tetraphenyl porphyrinic guest molecules.[11] More recently, molecular modeling coupled with powder X-ray diffraction (XRD) has suggested an alternation of nitrate and porphyrin containing interlayer domains for partially exchanged MgAl-NO_3/TSPP samples.[22] The $[TSPP]^{4-}$ anions are tilted with respect to the hydroxide layer of about 50–60°.

Electrochemical behaviour of metalloprophyrins has also been widely investigated because of their rich redox and electrocatalytic properties.[8,36] Such electrocatalytic properties associated with the possibility of immobilizing on different matrices have been exploited for the development of amperometric and voltammetric sensors.[37,38] However, to the best of our knowledge, only two papers have been devoted to the electrochemical study of porphyrins immobilized on LDH. So far in 1993, Gaillon *et al.* were the first to study the electrochemical behaviour of MgAl-MnTSPP.[25] More recently, ordered ultrathin films were built on electrode surfaces by the layer-by-layer self-assembled technique using FeTSPP and CoAl LDH nanosheets.[28] These modified electrodes exhibit electrocatalytic behaviour with hydrogen peroxide. Finally, Shich *et al.* in 2002 suggested that an electron transfer between interlayer Fe^{III} cations of MgFe-LDH and intercalated CoTSPP could occurred spontaneously during the exchange process.[27]

In the present work, we describe the synthesis, the structural characterization and the electrochemical behaviour of Zn_2Cr-ZnTSPP and Zn_2Cr-FeTSPP hybrid LDH materials. The intercalation of porphyrins in ZnCr-LDH has never been reported so far. Although, the particularly good stability of Zn_2Cr-LDH host over a wide pH range allows electrochemical applications of these hybrid materials in both neutral and acid buffer solutions. Electrocatalytic properties of Zn_2Cr-FeTSPP for the reduction of oxygen, hydrogen peroxide and nitrite were investigated by cyclic voltammetry.

2. Experimental

2.1. Material

Free base 5,10,15,20-tetrakis(4-sulfonatophenyl)porphyrin (TSPP) was purchased from Sigma-Aldrich. Hydrogen peroxide (H_2O_2) solutions (from Sigma-Aldrich) were freshly prepared before being used. $Na_2HPO_4{\cdot}10H_2O$, NaH_2PO_4, $Zn(NO_3)_2{\cdot}6H_2O$ and $Cr(NO_3)_3.9H_2O$ were purchased from Acros. Iron(III) porphyrin (FeTSPP) was obtained by iron insertion into the free-base porphyrin ligand using ferrous chloride tetrahydrate in DMF. Purification was performed by colum chromatography on sephodex, using deionized water as eluent.[12] Zinc(II) porphyrin (ZnTSPP) was prepared by stirring *p*TSPP with an equimolar amount of Zn^{2+} for 1 h.[23]

Hybrid LDH materials, noted as Zn_2Cr-ZnTSPP and Zn_2Cr-FeTSPP, were prepared by coprecipitation by adapting the method for small quantities of materials. Typically, a mixed aqueous solution of $Zn(NO_3)_2{\cdot}6H_2O$ and $Cr(NO_3)_3{\cdot}9H_2O$, with a Zn^{2+}/Cr^{3+} molar ratio $R = 2$, and a total concentration of metallic cations of 0.1 M, was introduced with a constant flow (0.007 mL min^{-1}) into a reactor containing metalloporphyrins (ZnTSPP or FeTSPP), noted MTSPP hereafter, in aqueous solution stirred under nitrogen atmosphere. The amount of MTSPP corresponded to twofold the number of mole required for a stoichiometric 100% exchange reaction (6–8 mM in 10 ml). The pH was maintained constant during the coprecipitation process at a value of 6.25 by simultaneous addition of a 0.2 M NaOH solution. After an aging time of 24 h, Zn_2Cr-MTSPP solid products were recovered by centrifugation and washed twice with decarbonated water.

It is noteworthy that aqueous solutions of FeTSPP are characterized by a pH-dependent equilibrium of monomers and dimeric species.[39–42] Indeed, this metalloporphyrin exists as monomers in acidic solution and may form μ-oxo dimers in basic solutions with an apparent pK value of 7.8.[42] The equilibrium, which depends on the pH of the solution but also on its ionic strength and on the porphyrin concentration, can be written as follows:

$$2[Fe(H_2O)TSPP]^{3-} \rightleftarrows [TSPPFe\text{-}O\text{-}FeTSPP]^{8-} + H_2O + 2H^+ \quad (1)$$

where iron(III) is pentacoordinated in a high spin state. One can also note that hexacoordinate iron $Fe(H_2O)_2TSPP$ or intermediate hydroxo species $[Fe(OH)_nTSPP]^{4-}$ with $n = 1$ or 2 have been also reported.[40–42] Since the coprecipitation of Zn_2Cr-FeTSPP LDH was carried out at pH 6.25 in an aqueous solution of 8 mM FeTSPP, the formation of such dimeric forms is highly probable. Therefore in order to specify species present in the solution under our synthesis conditions, the UV-Vis behaviour of an aqueous solution of FeTSPP (60 μM) was examined as a function of the pH and the ionic strength (see ESI, Fig. ESI1†). In water at pH 6.3, the maximum adsorption is at 394 nm with a shoulder at 415 nm (Soret band) and the smaller bands are at 500 and 529 nm (Q bands). In 0.1 M buffer solutions, at pH 6.25, we observed a red shift of the bands while at pH 7.5, the formation of the deep green μ-oxo dimer was observed characterized by a Soret band at 407 nm and Q bands at 566 and 610 nm, as reported in the literature.[42] In the copreciptation medium, the porphyrin concentration is *ca.* 130 times higher as compared to the concentration used for these above UV-Vis measurements. This concentration effect together with the increase in salt concentration during the coprecipitation process are expected to shift equilibrium (1) further towards dimer formation.[40,41] Moreover, $[TSPPFe\text{-}O\text{-}FeTSPP]^{8-}$ exhibits a high negative charge compared to $[Fe(H_2O)TSPP]^{3-}$ which may also be in

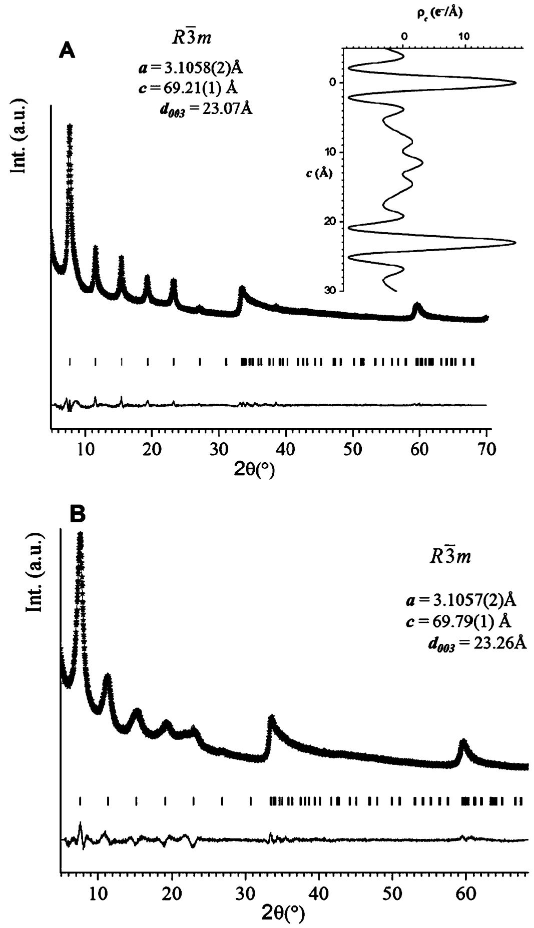

Fig. 1 Results of the profile analysis of XRPD patterns for (a) Zn_2Cr-ZnTSPP and (b) Zn_2Cr-FeTSPP: experimental X-ray diffraction (dot), calculated (line), difference (bottom) and ticks giving the position of Bragg reflections in the space group $R\bar{3}m$. Profile parameters of the TCH function are for (a) Zn_2Cr-ZnTSPP: isotropic size parameter of Gaussian character (GauSiz = 0.056(1) and anisotropic size broadening described using IsizeModel16 (spherical harmonics coefficients: Y00 = 15.3(4), Y40 = −19.8(8), Y60 = 11.4(4), Y66+ = 1.9(1)) and for (b) Zn_2Cr-FeTSPP (GauSiz = 0.530(7); Y00 = 9.3(4), Y20 = −1.6(5), Y40 = −21.1(8), Y43- = −1.7(4), Y60 = 20.3(7), Y63 = −1.1(3), Y66+ = 5.3(3)). Inset: One-dimensional electron density ρ_c projection along the *c*-axis for Zn_2Cr-ZnTSPP.

favour of the intercalation of such dimers. In the present work, we will use notations $Fe(H_2O)_n$TSPP or $O(FeTSPP)_2$ for monomer or dimer species where the ionic charges have been omitted.

LDH-modified electrodes were prepared as films on a glassy carbon electrodes (A = 0.07 cm^2). Before use, the glassy carbon electrodes were polished with alumina slurry paste (0.05 μM) and rinsed with ethanol and distilled water. Hybrid LDH suspensions (4 mg ml^{-1}) were stirred under the darkness overnight before use. Aliquots (10 μl) of LDH samples were spread on the electrode surface and dried for 4 h.

2.2. Instrumentation

Powder X-ray diffraction patterns were recorded on X'Pert Pro diffractometer in Bragg Brentano geometry equipped with a X'-Celerator Scientific-RTMS detector and using Cu-Kα1/α1 radiation. The samples were placed on a Si low background sample holder and the measurements were performed in continuous scanning mode with the following setting conditions: beam mask = 10 mm, divergence slits = 1/32°, detector active length = 2.122°, scan range = 5–70°, steps size = 0.0167° and counting time = 850 s. Profile matching refinements were carried out with the Fullprof program[43] using the pseudo-Voigt profile function of Thompson, Cox and Hastings,[44] and included variation of lattice parameters and peak shape parameters. A LaB_6 standard was used to correct for instrumental broadening (U = 0.008(1), V = -0.009(1), W = 0.0036(5), Y = 0.033(2)). Owing to the platelet-like morphology of LDH particles, peak broadening was mainly attributed to anisotropic size effects; it was modeled in terms of spherical harmonics allowing the calculation of the coherent domain apparent size along different [*hkl*] crystallographic directions.[45]

FTIR-KBr spectra were recorded on a Nicolet 5700 (Thermo electron corporation) spectrometer. UV-Visible spectra were recorded using a Shimadzu UV-Vis 2001 PC spectrometer equipped with an integrating sphere. The samples were prepared as thin films on quartz plates following the same procedure as used to prepare thin films on electrodes.

Cyclic voltammetry experiments were carried out with a potentiostat Autolab PGSTAT100 connected to a cell (50 ml) with a three-electrode system, including an Ag/AgCl reference electrode, a platinum auxiliary electrode and a glassy carbon disk electrode (GCE) modified with LDH films as working electrode. All electrochemical experiments were performed in 0.1 M phosphate buffer solution (PBS pH 7 and 4.5) degassed by bubbling with argon for at least 30 min before starting the measurements.

3. Results and discussion

3.1. Structural characterization

It has been demonstrated many times that the coprecipitation method, by involving the *in situ* formation of LDH layers around species we wish to intercalate, facilitates the effective insertion of bulky porphyrin anions.[11,18,19,21,23] In the present case, the composition of LDH host based on Zn^{2+} and Cr^{3+} is peculiar for two reasons. First, the synthesis can be achieved at low coprecipitation pH; second, it occurs for a unique molar ratio equal to 2 whatever the proportion of di- and trivalent cations in the starting solution. This unique ratio is in favour of an ordered cation distribution within Zn_2Cr hydroxide layers as discussed by several authors.[46] This interlayer metal cation ordering is rather in favour to the ordering of the interlayer anions.

The XRD patterns of Zn_2Cr-ZnTSPP and Zn_2Cr-FeTSPP samples were indexed in the rhombohedral space group $R\bar{3}m$, typical for LDH systems (see ESI, Fig. ESI2†). Although Zn_2Cr-FeTSPP appears less crystalline than Zn_2Cr-ZnTSPP, the position of the **003*n*** basal lines is similar in both compounds indicating similar interlayer distances. Note that the lower signal-to-noise ratio seen in the case of Zn_2Cr-FeTSPP may also be attributed in part to iron fluorescence. The cell parameters given on Fig. 1(a) and (b) were obtained from the peak profile analysis and it should be noted that the spherical harmonics correction for an anisotropic peak broadening due to size effects was essential to reach a good fit. The values of the cell parameter a are identical (a = 3.1058(2) Å for Zn_2Cr-ZnTSPP and a = 3.1057(2) Å for Zn_2Cr-FeTSPP) and in total agreement with the formation of Zn_2Cr LDH host.[46] The values of the cell parameter c are also quite similar (c = 69.21(1) Å for Zn_2Cr-ZnTSPP and c = 69.79(1) Å for Zn_2Cr-FeTSPP) leading to an interlayer distance (d_{003}) of 23.07 Å for Zn_2Cr-ZnTSPP and 23.26 Å for Zn_2Cr-FeTSPP very close to the values reported for Zn_2Al-ZnTSPP[23] (23.00 Å) and Zn_2Al-FeTSPP[11] (22.95 Å) and thus consistent with the intercalation of the porphyrin molecules with the ring oriented perpendicularly with respect to the hydroxide layers.

The relatively good crystallinity of Zn_2Cr-ZnTSPP allowed us probing the structure of the interlayer space *via* the Fourier transform of the ***00l*** X-ray reflection intensities[47] and giving the one-dimensional electron-density distribution along the c-stacking axis presented in the inset of Fig. 1(a). This 1D plot is similar to that reported elsewhere for Zn_2Al-ZnTSPP[23] with the most intense peaks corresponding to the electron densities of the hydroxide layers, the maxima at the outer parts of the interlayer space are due to the sulfonate groups together with water molecules while the central maxima and the two peaks on each side arise from the porphyrin ring and zinc atom at the centre.

As said before, good profile refinements were obtained by assuming anisotropic broadening due to size effects. The broad features displayed by Zn_2Cr-FeTSPP suggest the presence of very small coherent domain sizes. From the refined spherical harmonics coefficients, it is possible to determine the volume-weighed domain size D_{hkl} in the direction parallel to the scattering vector q_{hkl}. Related to the platelet-like morphology of LDH particles, we focused on two directions [$\mathbf{003}\boldsymbol{n}$] and [**110**] indicative of the stacking thickness of LDH sheets and the platelet dimension in the plane, respectively. The lengths thus calculated were found to be 3/2 times larger for Zn_2Cr-ZnTSPP (thickness $D_{\mathbf{003}\boldsymbol{n}}$ of 120 Å and in-plane dimension $D_{\mathbf{110}}$ of 135 Å) than for Zn_2Cr-FeTSPP ($D_{\mathbf{003}\boldsymbol{n}}$ = 75 Å and $D_{\mathbf{110}}$ = 105 Å). One can also calculate the number of stacked interlayers $D_{\mathbf{003}\boldsymbol{n}}/d_{\mathbf{003}}$ leading to a value close to 5 in the case of Zn_2Cr-ZnTSPP and 3 for Zn_2Cr-FeTSPP.

This lower coherency for Zn_2Cr-FeTSPP is likely to result from structural strains accompanying FeTSPP intercalation. This idea of strain effect is reinforced by the fact that it was necessary to refine both Lorentzian and Gaussian size broadening to accurately model the XRD peak shape. In the case of Zn_2Cr-FeTSPP, the isotropic Gaussian size parameter was found 10 times larger than for Zn_2Cr-ZnTSPP. Such a mixed Gaussian and Lorentzian character more marked for Zn_2Cr-FeTSPP suggests the presence of both strain and size effects and we believe these strains are the result of the structural accommodation of aggregates oxo bridged diiron(III) complexes within the interlayer space of Zn_2Cr LDH. Indeed as discussed above in the experimental part, the dimerisation equilibrium of FeTSPP in aqueous homogeneous solution is expected to occur in the pH range 4–8.[40,42] It is interesting to note the synthesis pH of Zn_2Cr-FeTSPP *i.e.* 6.2 falls within this pH range. Accordingly, intercalated species in the as-prepared Zn_2Cr-FeTSPP sample are likely to be $O(FeTSPP)_2$ dimers.

When considering previous studies on FeTSPP intercalation into LDH system using the coprecipitation method, it is remarkable that whatever the M^{II}/M^{III} molar ratio ($2 \leq R \leq 4$) used during the synthesis, chemical and structural analyses of synthesized materials all display a R value close to 2.[11,12] Owing to the coprecipitation pH values applied (7.5 for Zn_RAl-LDH), one can reasonably assume in all cases the intercalation of $O(FeTSPP)_2$ dimers. By considering the Fe–O–Fe distance reported for $O(FeTPP)_2$, *i.e.* 3.516 Å with Fe–O–Fe angles close to linearity 176°,[48,49] one can estimate the surface area per unit charge (S_0) for a $O(FeTSPP)_2$ dimer, assuming an approximate parallelepiped shape of about 16.0 ×15.8 × 4.3 Å for FeTSPP macrocycle (as obtained from steric energy minimization using the MM2 method[50]) and a perpendicular orientation of the porphyrin ring with respect to LDH hydroxide layers. The value thus obtained equals 15.7 $Å^2/e^-$. The comparison with S_0 values of Zn_2Cr (25.3 $Å^2/e^-$) or Zn_2Al (25.0 $Å^2/e^-$) LDH hosts indicates a good surface compatibility.

Regarding Zn_2Cr-ZnTSPP, we cannot either exclude the formation of aggregates, particularly face-to-face dimers (H-aggregates), although UV-Vis spectra are weakly resolved (*videinfra*). Such a self-association is a frequently encountered phenomenon in porphyrin chemistry owing to intermolecular Van der Waals-like attractive forces between the molecules. This type of bonding being much weaker/longer and more flexible than bridging ligands certainly makes the structural assembly process with LDH host layers easier whatever the charge density of the hydroxide layers, as evidenced here by the high crystallinity of Zn_2Cr-ZnTSPP and that of Zn_RAl-ZnTSPP samples reported elsewhere.[23]

The presence of the organic anions within the LDH structure was confirmed by FTIR (see ESI, Fig. ESI3†) and UV-Vis spectroscopies. Fig. 2 compares the absorption spectra of free porphyrins (curves a and c) with those of intercalated complexes (curves b and d), prepared as thin films on quartz plates. We have verified that Zn_2Cr-LDH film does not absorb in the analyzed wavelength range (not shown). Spectra of solid metallo-porphyrins exhibit a strong adsorption band (Soret band) and only two Q bands. They are situated at 424, 561 and 603 nm for ZnTSPP and at 408, 578 and 621 nm for FeTSPP, as reported in the literature.[11,23] As previously

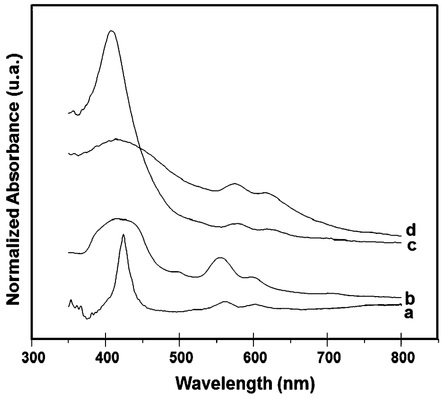

Fig. 2 Normalized UV-Vis spectra of thin films of ZnTSPP (a), Zn_2Cr-ZnTSPP (b) FeTSPP (c) and Zn_2Cr-FeTSPP (d).

observed in aqueous solution, the peak positions, reported for thin film prepared from aqueous solution of FeTSPP, do not correspond to the free monomer Fe(H_2O)$_n$TSPP in aqueous solution (Soret band at 394 nm and Q bands at 503 and 531 nm)[39,42]

A broadening of Soret bands is observed when porphyrins are intercalated in LDH interlayer, which is generally attributed to some degree of aggregation and stacking of the porphyrin molecules.[11] Zn_2Cr-ZnTSPP spectrum shows an intensive and broad Soret band centered at *ca.* 421 nm and two Q bands at 557 and 600 nm in agreement with ZnTSPP formation (Fig. 2, curve b). An additional absorption band less intense is observed at *ca.* 499 nm. It is not expected for monomeric ZnTSPP nor uncomplexed TSPP but more probably to J-aggregates of H_4TSPP.[51]Moreover for ZnTSPP, the Soret band broadening was less noticeable with Zn_2Al-ZnTSPP,[23] suggesting that this porphyrin is more favorable to aggregate when it is intercalated in Zn_2Cr-LDH than in Zn_2Al-LDH host structure. These results may be related to the cationic order in Zn_2Cr hydroxide layers strongly suggested by several authors. However it is difficult to determine unequivocally the nature of aggregates. The complex broad Soret band of Zn_2Cr-ZnTSPP is probably related to the presence, in different ratio, of H-aggregates (414 nm) and monomers (422 nm).[42]

For Zn_2Cr-FeTSPP, the Soret band is centered at *ca.* 415 nm and Q bands are situated at 575 and 619 nm (Fig. 2, curve d). As previously discussed, owing the coprecipitation pH value of Zn_2Cr-FeTSPP (pH 6.2), we can assume that the predominant intercalated species are oxo-bridged dimers O(FeTSPP)$_2$, corresponding to a red shift Soret band. This hypothesis seems to be confirmed with the presence of a vibration band at 873 cm^{-1} corresponding to the Fe–O–Fe antisymmetric stretching[39,49] (see ESI, Fig. ESI3†).

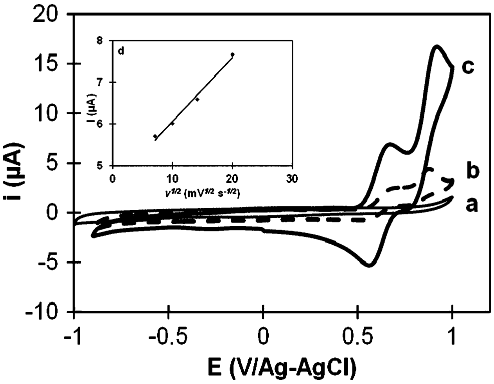

Fig. 3 Cyclic voltammograms recorded in the potential range between −1.0 and 1.0 V using Zn_2Cr-Cl/GCE (a) and Zn_2Cr-ZnTSPP/GCE at pH 7.0 (b) and pH 4.5 (c), inset shows the plot of the first anodic peak current *vs.* $\sqrt{\nu}$ (d) (0.1 M PBS under argon, ν = 50 mV s^{-1}).

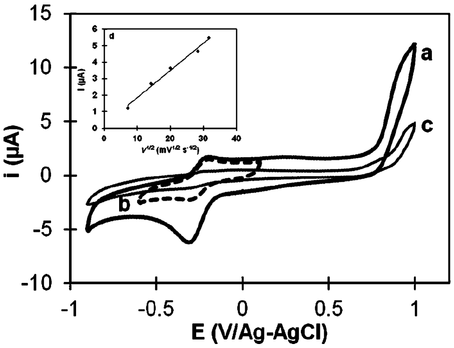

Fig. 4 Cyclic voltammograms of Zn_2Cr-FeTSPP/GCE recorded at pH 4.5 in the potential range between −1.0 and 1.0 V (a) or in the cathodic potential range (b), at pH 7.0 (c), inset shows the plot of Fe anodic peak current *vs.* $\sqrt{\nu}$ (d) (0.1 M PBS pH under argon, ν = 50 mV s^{-1}).

3.2. Electrochemical characterization

These hybrid materials can be examined by electrochemical methods such as cyclic voltammetry (CV). Electrochemical behaviour of porphyrins is known to be pH dependent. ZnCr-LDH host structure is stable in acid medium and we may assume that no dissolution of hybrid materials occurs at pH 4.5.[52] Cyclic voltammetry curves of glassy carbon electrodes (GCE) coated with 40 μg of ZnCr-LDH intercalated with Cl, ZnTSPP and FeTSPP were recorded in 0.1 M PBS at pH 7 and 4.5 under argon atmosphere, as shown in Fig. 3 and 4. Under these experimental conditions, Zn_2Cr-Cl LDH is not electroactive and the current base line is very similar to that obtained with a bare glassy carbon electrode (Fig. 3a).

When oxidation of Zn_2Cr-ZnTSPP was carried out at pH 7, two oxidation peaks appear on the voltammogram at +0.65 and +0.90 V (Fig. 3b). In acid medium (pH 4.5), the electrochemical signal increases and the first peak, situated at $E_{1/2}$ = +0.60 V, becomes more reversible (Ip_a/Ip_c = 1.24, ΔE_p = 80 mV) (Fig. 3c). Since Zn cation is not electroactive, these oxidation processes occur on the porphyrin ring, leading to the successive formation of the radical cation Zn[TSPP$^{+\bullet}$] and dication Zn[TSPP^{2+}].[53] The attenuation of cyclic voltammetric curves at neutral pH can be interpreted in terms of slowing of the kinetics for heterogeneous charge transfer, depending on the nature of axial ligands on metal.[36] Indeed, the equilibrium distribution of porphyrins species depends on the pH, with a predominant concentration of Zn(H_2O)$_2$TSPP, Zn(H_2O)(OH)TSPP and Zn(OH)$_2$TSPP at pH 5.2, 6.2 and 8.5, respectively.[54] Moreover as suggested by Su *et al.*, the radical cation Zn[TSPP$^{+\bullet}$], which can be also formed by a dismutation reaction between the dication Zn[TSPP^{2+}] and the reduced macrocycle Zn[TSPP], is particularly stable at pH 4.[53] This fact can explain the enhanced reversibility of the first electron transfer at pH 4.5. The current intensity of the first anodic peak is proportional to the square root of the scan rate ($\sqrt{\nu}$) in the 50–400 mV s^{-1} range, indicating that the oxidation of [TSPP] macrocycle inside the LDH host is governed by a diffusional process, in which electrolyte ions play a key role in the charge balancing effect[52,55,56] (Fig. 3d). The number of electroactive species (n*) in the film is obtained by integration of the area under the first anodic peak recorded at slow scan rate (ν = 10 mV s^{-1}, n^* ≈2 × 10^{-10} mole). This value corresponds to the lowest value found for other LDH containing redox active anions, such as anthraquinone sulfonates, ferrocene sulfonates or 2,2′-azino-bis(3-ethylbenzthiazoline-6-sulphonate) (0.25–2 × 10^{-9} mole).[52,55–57] Indeed, we have previously shown that only 2 to 20% of intercalated anions in the LDH-modified electrodes are electroactive, depending on their

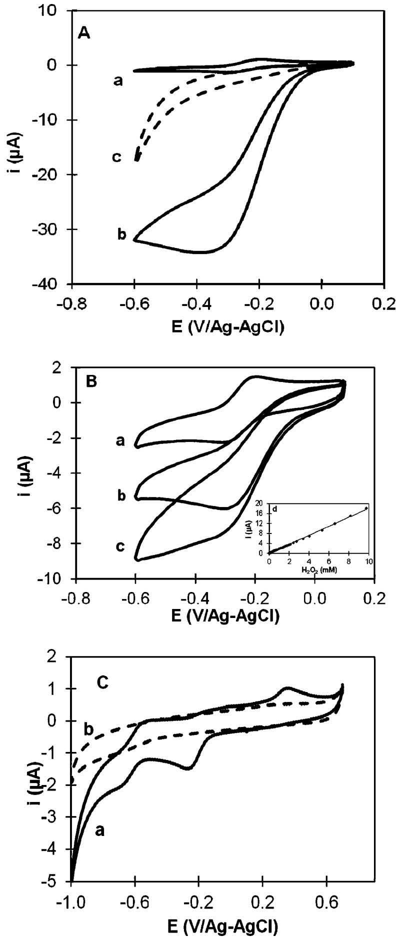

Fig. 5 (**A**) Cyclic voltammograms of Zn_2Cr-FeTSPP/GCE recorded under argon atmosphere (a), under saturated O_2 atmosphere (b) and bare GCE under saturated O_2 atmosphere (c). (**B**) Cyclic voltammograms of Zn_2Cr-FeTSPP/GCE in the presence of 0 (a), 0.4 (b) and 0.8 mM H_2O_2 (c), H_2O_2 calibration curve recorded at −0.4 V (d). (**C**) Cyclic voltammograms recorded at Zn_2Cr-FeTSPP/GCE (a) and bare GCE (b) in the presence of 0.2 mM $NaNO_2$. (Experimental conditions: 0.1 M PBS pH 4.5 under argon, ν = 50 mV s^{-1}.)

electrochemical accessibility.[52,55–57] In the present case, the theoretical amount of intercalated porphyrin tetrasulfonate anions is at least two or four times lower than disulfonate or monosulfonate anions. Moreover, these macrocyclic molecules must be in a specific coordination to be electroactive.

Finally in order to study the reversibility of this pH effect and to confirm the good stability of the ZnCr-LDH coating in acidic medium, the same modified electrode was tested successively in acidic, neutral and acidic media. The Zn_2Cr-ZnTSPP/GCE was stabilized in each medium during 20 cycles (see Fig. ESI4A†). The first CV curve is restored by soaking back the electrode in PBS at pH 4.5. Moreover, this signal remains unchanged after a further 2 h soaking in PBS pH 4.5.

The electrochemical behaviour of free or immobilized FeTSPP is known to be pH dependent depending on the nature axial ligands H_2O, OH^-, O^{2-} on the metal.[40,58–63] From DRX and UV-Vis measurements, we can assume that oxo-bridged dimers $O(FeTSPP)_2$ are present within the interlayer space of Zn_2Cr-LDH host matrix (*vide supra*). Since iron complexed in this dimer configuration is known to be electrochemically silent,[40,59,63] the electrochemical measurements were done at a pH value of 4.5. Under this acidic condition, one can expect that $Fe(H_2O)_n$TSPP species should be present in the LDH host.[42] Hence, the cyclic voltammogram displays a reversible peak system at $E_{1/2} = -0.24$ V, which corresponds to the $Fe^{III}(H_2O)_n$TSPP/$Fe^{II}(H_2O)_n$TSPP redox couple as reported for FeTSPP in aqueous acid solution (−0.23 V).[40,60,61] A further oxidation occurs at +0.90 V which corresponds to the porphyrin ring based oxidation (Fig. 4).[40,60] This oxidation process is irreversible, probably due to the formation of iron(III)isoporphyrin by a nucleophilic attack on the porphyrin radical cation generated in the oxidation step.[58,60] This by-product can be reduced in the reverse scan that can explain the higher reduction current observed in the cyclic voltammetry curve recorded in the large potential range (Fig. 4, curve b). Hence, the reversibility of the Fe^{III}/Fe^{II} electrochemical signal increases ($Ip_a/Ip_c = 1.2$, $\Delta E_p = 76$ mV) when scanning only in the cathodic potential range (Fig. 4, curve b). At pH 7, these reversible peaks disappear but the oxidation wave remains with a slightly lower intensity (Fig. 4, curve c). As previously observed with Zn_2Cr-ZnTSPP, this pH effect is reversible, the same CV was recovered after cycling successively the same modified electrode in both PBS (see Fig. ESI4B). The intensity of oxidation peak of Fe(II) recorded at pH 4.5 increases with $\sqrt{\nu}$, the electron transfer is under diffusion control (Fig. 4d). We have calculated the amount of electroactive species present within the film at pH 4.5 by integration of the oxidation peak of Fe^{II} at low scan rate (ν = 5 mV s^{-1}). This amount, which should correspond to monomer species, was found to be also very low ($n^* \approx 1 \times 10^{-10}$ mole).

Iron(III) porphyrins are known as catalysts for the electrochemical reduction of molecular oxygen, hydrogen peroxide and nitrite.[40,60,62,64,65] The cyclic voltammograms shown in Fig. 5A have been recorded at Zn_2Cr-FeTSPP modified electrode in electrolyte solution (pH 4.5) saturated with argon (curve a) or oxygen (curve b). As expected, the reversible redox signal observed in deaerated solution was masked by an intense catalytic redox wave under oxygen saturated atmosphere. The intensity of this electrocatalytic wave can be compared to the current peak corresponding to the direct reduction of oxygen at a bare glassy carbon electrode (curve c). Similarly when H_2O_2 is added in the deaerated PBS, an increase in the reduction peak is observed (Fig. 5B).An amperometric response to successive additions of H_2O_2 was recorded at −0.4 V using a Zn_2Cr-FeTSPP/GC rotating disk electrode (A = 0.196 cm^2). A linear variation of the reduction current as a function of H_2O_2 concentration was obtained between 1×10^{-5} to 1×10^{-2} M. This shows that Zn_2Cr-FeTSPP has also a peroxidase-like activity for the reduction of H_2O_2.[60] As previously reported in the literature for FeTSPP dissolved in buffer solution or immobilized in polypyrrole,[40,62] the presence of nitrite caused a drastic modification of the voltammograms (Fig. 5C). In 0.2 mM nitrite solution the cyclic voltammogram shows a wave for the reduction of Fe^{III} at −0.26 V but the return wave becomes quasi-unobservable, except at low scan rate (ν = 5 mV s^{-1}). A second reduction wave occurs at −0.68 V and in the reverse anodic scan a new wave appears at +0.34 V. It should be noted that there is no disproportion of nitrite at pH > 4 and cyclic voltammogram recorded at a bare glassy carbon electrode shows a negligible reduction current in nitrite solution (Fig. 5C, curve b). This suggests that nitrite may interact with intercalated FeTSPP. This phenomenon is reversible, since when the same electrode was cycled in buffer solution, the reversible Fe^{III}/Fe^{II} signal appears again. As reported in the literature, interaction between nitrite and iron porphyrins exists through the reduction of metal centre followed by a multi-electron catalytic process to form iron-nitrosyl intermediates ($Fe^{II}[NO^{\bullet}TSPP]$ and $Fe^{II}[NO^{-}TSPP]$), the anodic peak at 0.34 V corresponding to $Fe^{II}[NO^{\bullet}TSPP]/\ Fe^{II}[NO^{+}TSPP]$ oxidation[40,62,65]

4. Conclusions

Metallo-porphyrin anionic complexes ZnTSPP and FeTSPP were successfully intercalated between Zn_2Cr-LDH layers using coprecipitation method at constant pH 6.2. Careful structural and electrochemical characterizations of hybrid materials were conducted, showing the intercalation of guest molecules as a H aggregates in the case of Zn_2Cr-ZnTSPP and an oxo-bridged diron(III) complexes in the case of Zn_2Cr-FeTSPP. While a small contribution from monomers (1%) can be taken into account in the electrochemical responses at pH 4.5. In both cases, we observed a perpendicular arrangement of the porphyrin ring with respect to the LDH layers. Finally, iron species in Zn_2Cr-FeTSPP exhibit an electrocatalytic activity for the reduction of oxygen, hydrogen peroxide and nitrite. Although the electroactivity of these hybrid materials remains low, we anticipate that such Zn_2Cr LDH phases, stable at low pH, will find applications as sensors or photocatalysts.

Acknowledgements

This work was supported by the CMCU (06/S1207) and MIRA programs. We thank N. Caperaa for her technical assistance, S. Therias (LPMM UMR 6505, Clermont-Ferrand) for experimental facilities and K. Lang, Institute of Inorganic Chemistry of the Academy of Sciences of the Czech Republic, for fruitful discussion on UV-Vis absorption data.

References

1 J.-H. Choy, S.-J. Choi, J.-M. Oh and T. Park, *Appl. Clay Sci.*, 2007, **36**, 122–132.

2 U. Costantino, V. Ambrogi, M. Noccheti and L. Perioli, *Microporous Mesoporous Mater.*, 2008, **107**, 149–160.

3 C. Forano, S. Vial and C. Mousty, *Curr. NanoSci.*, 2006, **2**, 283–294.

4 F. Li and X. Duan, in *Structure and Bonding*, ed. D. M. P. Mingos, Springer-Verlag, Berlin Heidelberg, 2006, pp. 193–223.

5 M. H. Valkenberga and W. F. Houmllderic, *Catal. Rev. Sci. Eng.*, 2002, **44**, 321–374.

6 H. Nobukuni, Y. Shimazaki, H. Uno, Y. Naruta, K. Ohkubo, T. Kojima, S. Fukuzumi, S. Seki, H. Sakai, T. DHasobe and F. Tani, *Chem.–Eur. J.*, 2010, **16**, 11611–11623.

7 P. Banerjee, D. Conklin, S. Nanayakkara, T.-H. Park, M. J. Therien and D. A. Bonnell, *ACS Nano*, 2010, **4**, 1019–1025.

8 J. H. Zagal, S. Griveau, K. I. Ozoemena, T. Nyokong and F. Bedioui, *J. Nanosci. Nanotechnol.*, 2009, **9**, 2201–2214.

9 I. Y. Park, K. Kuroda and C. Karo, *Chem. Lett.*, 1989, 2057–2058.

10 T. J. Pinnavaia, M. Chibwe, V. R. L. Constantino and S. K. Yun, *Appl. Clay Sci.*, 1995, **10**, 117–129.

11 M. Halma, A. K. Dias de Freitas Castro, C. Taviot-Gueho, V. Prevot, C. Forano, F. Wypych and S. Nakagaki, *J. Catal.*, 2008, **257**, 233–243.

12 M. Halma, A. K. Dias de Freitas Castro, V. Prévot, C. Forano, F. Wypych and S. Nakagaki, *J. Mol. Catal. A: Chem.*, 2009, **310**, 42–50.

13 L. Barloy, J. P. Lallier, D. Mansuy, J. Piffard, M. Tournoux, J. B. Valim and W. Jones, *New J. Chem.*, 1992, **16**, 71–80.

14 M. Halma, F. Wypych, S. M. Drechsel and S. Nakagaki, *J. Porphyrins Phthalocyanines*, 2002, **6**, 502–513.

15 S. Takagi, M. Eguchi, D. A. Tryk and H. Inoue, *J. Photochem. Photobiol., C*, 2006, **7**, 104–126.

16 K. Lang, P. Bezdicka, J. L. Bourdelande, J. Hernanado, I. Jirka, E. Kafunkova, F. Kovanda, P. Kubat, J. Mosinger and A. M. Wagnerova, *Chem. Mater.*, 2007, **19**, 3822–3829.

17 K. Lang, P. Kubat, J. Mosinger, J. Bujdak, M. Hof, P. Janda, J. Sykora and N. Iyi, *Phys. Chem. Chem. Phys.*, 2008, **10**, 4429–4434.

18 S. Y. Ryu, M. Yoon, J. H. Choy, S. H. Hwang, A. Frube, T. Asahi, H. Masuhara and B. Kor, *Chem. Soc*, 2003, **24**, 446–452.

19 E. Káfuňková, K. Lang, P. Kubát, M. Klementová, J. Mosinger, M. Šlouf, A.-L. Troutier-Thuilliez, F. Leroux, V. Verney and C. Taviot-Guého, *J. Mater. Chem.*, 2010, **20**, 9423–9432.

20 F. Kovanda, E. Jindová, K. Lang, P. Kubát and Z. Sedláková, *Appl. Clay Sci.*, 2010, **48**, 260–270.

21 S. Bonnet, C. Forano, A. de Roy and J.-P. Besse, *Chem. Mater.*, 1996, **8**, 1962–1968.

22 P. Kovar, M. Pospisil, E. Kafunkova, K. Lang and F. Kovanda, *J. Mol. Model.*, 2009, **16**, 223–233.

23 E. Káfuňková, C. Taviot-Gueho, P. Bezdika, M. Klementov, P. Kov, P. Kubt, J. Mosinger, M. Pospil and K. Lang, *Chem. Mater.*, 2010, **22**, 2481–2480.

24 A. Píšková, P. Bezdička, D. Hradil, E. Káfuňková, K. Lang, E. Večerníková, F. Kovanda and T. Gryga, *Appl. Clay Sci.*, 2010, **49**, 363–371.

25 L. Gaillon, F. Bedoui, J. Devynck and P. Battioni, *J. Electroanal. Chem.*, 1993, **347**, 435–442.

26 Z. Tong, S. Tetsuya and T. Katsuhiko, *Mater. Lett.*, 2003, **57**, 2258–2261.

27 T. Shichi, Z. Tong, S. Hirai and K. Takagi, *Chem. Lett.*, 2002, 834–835.

28 M. Shao, J. Han, W. Shi, M. Wei and X. Duan, *Electrochem. Commun.*, 2010, **12**, 1077–1080.

29 S. Nakagaki, M. Halma, A. Bail, C. Guadalupe, A. Gregoria, C. Guadalupe and F. Wypych, *J. Colloid Interface Sci.*, 2005, **281**, 417–423.

30 Z. Tong, T. Shichi, G. Zhang and K. Takagi, *Res. Chem. Intermed.*, 2003, **29**, 335–341.

31 H. Tahaya, A. Ogata, T. Kuwahara, S. Ogata, M. Karasu, J.-i. Kadokawa and K. Chiba, *Microporous Mater.*, 1996, **7**, 151–158.

32 C. A. S. Barbosa, A. M. D. C. Ferreira and V. R. L. Constantino, *Eur. J. Inorg. Chem.*, 2005, 1577–1584.

33 F. Wypych, G. A. Bubniak, M. Halma and S. Nakagaki, *J. Colloid Interface Sci.*, 2003, **264**, 203–207.

34 F. Wypych, A. Bail, M. Halma and S. Nakagaki, *J. Catal.*, 2005, **234**, 431–437.

35 T. Yui, T. Kameyama, T. Sasaki, T. Torimoto and K. Takagi, *J. Porphyrins Phthalocyanines*, 2007, **11**, 428–433.

36 K. M. Kadish and E. Van Caemelbecke, *J. Solid State Electrochem.*, 2003, **7**, 254–258.

37 M. Biesaga, K. Pyrzynska and M. Trojanowicz, *Talanta*, 2000, **51**, 209–224.

38 J. F. Van Staden and R. I. Stefan-Van Staden, *Talanta*, 2010, **80**, 1598–1605.

39 E. B. Fleischer, J. M. Palmer, T. S. Srivastava and A. Chatterjee, *J. Am. Chem. Soc.*, 1971, **93**, 3162–3167.

40 M. H. Barley, K. J. Takeuchi and T. J. Meyer, *J. Am. Chem. Soc.*, 1986, **108**, 5876–5885.

41 A. A. El-Awady, P. C. Wilkins and R. G. Wilkins, *Inorg. Chem.*, 1985, **24**, 2053–2057.

42 S. C. M. Gandini, V. E. Yushmanov and M. Tabak, *J. Inorg. Biochem.*, 2001, **85**, 263–277.

43 T. Roisnel and J. Rodriguez-Carvajal, *Mater. Sci. Forum*, 2001, **378–381**, 118–123.

44 P. Thompson, D. E. Cox and J. B. Hastings, *J. Appl. Crystallogr.*, 1987, **20**, 79–83.

45 M. Jarvinen, *J. Appl. Crystallogr.*, 1993, **26**, 525–531.

46 H. Roussel, V. Briois, E. Elkaim, A. de Roy and J. P. Besse, *J. Phys. Chem. B*, 2000, **104**, 5915–5923, and references therein.

47 M. S. Whittingham and A. Jacobson, *Intercalation Chemistry*, Academic Press, New York, 1982.

48 P. N. Swepston and J. A. Ibers, *Acta Crystallogr., Sect. C: Cryst. Struct. Commun.*, 1985, **41**, 671–673.

49 E. B. Fleischer and T. S. Srivastava, *J. Am. Chem. Soc.*, 1969, **91**, 2403–2405.

50 CS Chem3D Ultra Program—Cambridge Soft Corporation, CS Chem3D Ultra 5.0: Ultimate Modeling, Visualization and Analysis, (1998), Cambridge.

51 J. Ribo, J. Crusats, J. A. Farrera and M. L. Valero, *Chem. Commun.*, 1994, 681–682.

52 A. Zebda, S. Tingry, C. Innocent, S. Cosnier, C. Forano and C. Mousty, *Electrochim. Acta*, 2011, DOI: 10.1016/j.electracta.2010.1001.1101.

53 Y. O. Su, D. Kim and T. G. Spiroa, *J. Electroanal. Chem.*, 1988, **246**, 363–371.

54 A. Farajtabar, F. Gharib and N. Safari, *J. Chem. Eng. Data*, 2008, **53**, 350–354.

55 S. Therias, C. Mousty, C. Forano and J. P. Besse, *Langmuir*, 1996, **12**, 4914–4920.

56 C. Mousty, C. Forano, S. Fleutot and J. C. Dupin, *Electroanalysis*, 2009, **21**, 399–408.

57 C. Mousty, S. Therias, C. Forano and J.-P. Besse, *J. Electroanal. Chem.*, 1994, **374**, 63–69.

58 C. Degrand, B. Limoges, A.-M. Martre and B. Schollhorn, *Analyst*, 2001, **126**, 887–891.

59 S.-M. Chen, *J. Electroanal. Chem.*, 1996, **407**, 123–130.

60 M. F. Zipplies, W. A. Lee and T. C. Bruice, *J. Am. Chem. Soc.*, 1986, **108**, 4433–4445.

61 D. Rong and T. E. Mallouk, *Inorg. Chem.*, 1993, **32**, 1454–1459.

62 F. Bedioui, Y. Bouhier, C. Sorel, J. Devynck, L. Coche-Guerente, A. Deronzier and J.-C. Moutet, *Electrochim. Acta*, 1993, **38**, 2485–2491.

63 S.-M. Chen, *Electrochim. Acta*, 1997, **42**, 1663–1673.

64 T. Sawaguchia, T. Matsuea, K. Itaya and I. Uchida, *Electrochim. Acta*, 1991, **36**, 703–708.

65 F. Bedioui, S. Trevin, V. Albin, M. G. Gomez Villegas and J. Devynck, *Anal. Chim. Acta*, 1997, **341**, 177–185.